

N. Khoshbakht,<sup>1</sup> P. L. Clouston,<sup>2</sup> S. R. Arwade,<sup>3</sup> and A. C. Schreyer<sup>2</sup>

## Evaluation of ASTM D5764 Dowel Connection Tests for Laminated Veneer Bamboo (LVB)

### Reference

N. Khoshbakht, P. L. Clouston, S. R. Arwade, and A. C. Schreyer, "Evaluation of ASTM D5764 Dowel Connection Tests for Laminated Veneer Bamboo (LVB)," *Journal of Testing and Evaluation* 47, no. 4 (July/August 2019): 2717–2736. <https://doi.org/10.1520/JTE20180385>

### ABSTRACT

The ASTM [D5764](#) standard, *Standard Test Method for Evaluating Dowel-Bearing Strength of Wood and Wood-Based Products*, for testing dowel connections provides a procedure for measuring the dowel bearing strength of wood and wood-based products. Laminated veneer bamboo (LVB) is a new building product that is employed in similar sizes and applications as dimensional lumber. Being new, more research is needed to understand the key factors and fundamental failure mechanisms that occur in LVB dowel connections to help ensure safe standards for further LVB product adoption and design. This study develops three-dimensional bilinear finite element models for half- and full-hole specimens in accordance with ASTM [D5764](#) when loaded in compression parallel to the grain. The models simulate LVB fracture initiation due to shear stresses in the dowel joint by incorporating frictional stresses in the contact region between a steel bolt and LVB. The model also predicts displacement at failure, which is validated through comparison with experimental results: the material fails at 1 and 1.18 mm displacement loading parallel to the grain for half- and full-hole specimens, respectively. It is found that, despite the higher load-bearing capacity (strength) of the half-hole specimen, both specimens fail at approximately the same displacement because of in-plane shear stresses. This article clarifies the complex interactive state of in-plane shear, tension perpendicular to the grain, and compression parallel-to-grain stresses using the Tsai–Wu failure criterion in the critical zone beneath the bolt hole for half- and full-hole specimens. These findings suggest that care should be taken to select a test method that captures the performance of LVB dowel joints because of different failure mechanisms that occur for full- and half-hole specimens.

### Keywords

full-hole test, half-hole test, dowel connection, embedment strength, failure behavior, finite element analysis, laminated veneer bamboo, friction, Tsai–Wu

Manuscript received June 5, 2018; accepted for publication October 10, 2018; published online February 19, 2019.

<sup>1</sup> Department of Environmental Conservation, University of Massachusetts Amherst, 551 N. Pleasant St., Amherst, MA 01003-2901, USA (Corresponding author), e-mail: [nkhoshbakht@umass.edu](mailto:nkhoshbakht@umass.edu), <https://orcid.org/0000-0003-3825-1334>

<sup>2</sup> Department of Environmental Conservation, University of Massachusetts Amherst, 551 N. Pleasant St., Amherst, MA 01003-9293, USA

<sup>3</sup> Department of Civil and Environmental Engineering, University of Massachusetts Amherst, 130 Natural Resources Rd., Amherst, MA 01003, USA

## Introduction

Laminated veneer bamboo (LVB) is employed in the same manner as engineered lumber, typically as posts and beams. Being a relatively new building material in North America, it was only recently added to the material testing standard ASTM D5456, *Standard Specification for Evaluation of Structural Composite Lumber Products*, in 2017.<sup>1</sup> This standard recommends the test same protocols for LVB and wood alike. Recent research, however, on LVB dowel connections<sup>2,3</sup> has indicated that bamboo lumber exhibits different failure mechanisms than softwood lumber, especially for the dowel bearing response. This finding raises questions about the appropriateness of adopting a wood standard for LVB.

A handful of research studies compare standard test methods and specimens for the dowel bearing response, but their focus has primarily been softwood species. For example, Santos et al.<sup>4</sup> used maritime pinewood and did a comparison between two standard test methods: BS EN 383, *Timber Structures. Test Methods. Determination of Embedment Strength and Foundation Values for Dowel Type Fasteners*,<sup>5</sup> and ASTM D5764, *Standard Test Method for Evaluating Dowel-Bearing Strength of Wood and Wood-Based Products*,<sup>6</sup> one with a full-hole specimen and the other with a half-hole specimen, as described in the respective standards. The authors concluded that the embedment strength measured for both standards are essentially the same. They also found a positive relationship between the embedment strength and density following the ASTM D5764 method. It is noteworthy that, according to their outcomes, in the BS EN 383 method, the average specimen displacement at yield was nearly twice as much as that of the specimens following the ASTM D5764 method for the longitudinal compression test because of the proposed half-hole geometry.<sup>4</sup>

Similarly, but using spruce specimens, Franke and Magniere<sup>7</sup> evaluated different dowel embedment testing methods and highlighted the major differences between standards. The authors showed that the variation in the specimen geometry and loading and differences in the evaluation method of finding stiffness and bearing strength affect the embedment strength significantly.

Importantly, recent work by Reynolds et al.<sup>2</sup> and Khoshbakht et al.<sup>3</sup> revealed a meaningful difference in failure mechanism between Moso LVB dowel joints and timber dowel joints: both studies found that high shear stresses around the bolt hole were primarily responsible for bamboo dowel failure, while tensile stresses perpendicular to the grain were the primary cause of failure in timber joints – the latter also being affirmed by Reynolds et al.<sup>2</sup>

ASTM D5764 recommends using half-hole specimens “unless the specimens tend to split before the completion of the test,” in which case the full-hole test is required.<sup>6</sup> To the authors’ knowledge, the effect of using these different test setups (specifically full- versus half-hole specimens) on the dowel failure behavior of LVB and other similar hardwood materials has not yet been fully investigated. In this article, we evaluate the ASTM method specifically, with regards to the embedment test procedure for LVB specimens, to recommend an appropriate test method for LVB dowel joints. We base our work on experimental data and nonlinear finite element (FE) simulations by describing the behavior of Moso LVB dowel connections under compressive loading using orthotropic material properties for both the full- and half-hole arrangements. In so doing, we aim to provide insight into LVB failure mechanisms, which can further support the development of codes and standards for bamboo connection detailing and design to facilitate the worldwide adoption of bamboo in modern construction.

One additional factor that has not been considered in the standards for dowel bearing properties is the surface roughness of the dowel hole. This effect has been addressed in past studies<sup>8,9</sup> and recent papers<sup>10</sup> and is shown to be a critical factor in determining the load-bearing capacity of the connection. The foci of these studies, however, are softwood species. Hence, in this article, the effect of surface roughness on the load-bearing capacity of the LVB dowel joint will also be addressed.

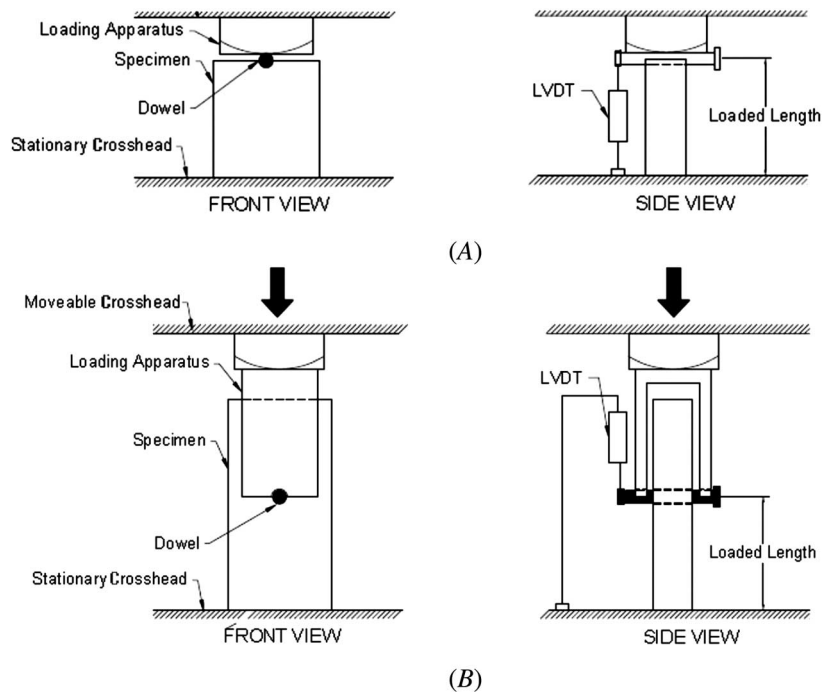
## Embedment Test Setup

Prior to conducting the embedment test, the material properties of LVB (shear, tension, and compression parallel to and perpendicular to the grain), were experimentally determined per ASTM D143, *Standard Test Methods for Small Clear Specimens of Timber*.<sup>11</sup> These values were necessary as input parameters for subsequent FE studies of

**FIG. 1**

Embedment test setup based on ASTM D5764:

(A) half-hole and  
(B) full-hole test.



the dowel joints. In the experimental tests, the commercially available LVB boards used were made from Moso bamboo (*Phyllostachys heterocycla* var. *pubescens*) procured by the company Lamboo® Technologies. This LVB material consists of 6.4 mm by 19 mm bamboo culm strips that are bonded together with an ANSI/HPVA Type 1 adhesive. The boards were conditioned for a minimum of 2 months in constant ambient environmental conditions. The mean moisture content of the samples was 5.4 %.

The material preparation and test procedure for the evaluation of embedment properties followed ASTM D5764, which is designed for testing a single dowel joint of wood-based products (see fig. 1). The sample consisted of 10 replications for each full- and half-hole arrangement as determined by ASTM D2915, *Standard Practice for Evaluating Allowable Properties for Grades of Structural Lumber*.<sup>12</sup> An MTS3000 testing machine was utilized in combination with a linear variable differential transformer (LVDT) to measure the displacement at the contact surface of the dowel joints to obtain the load-displacement curves.

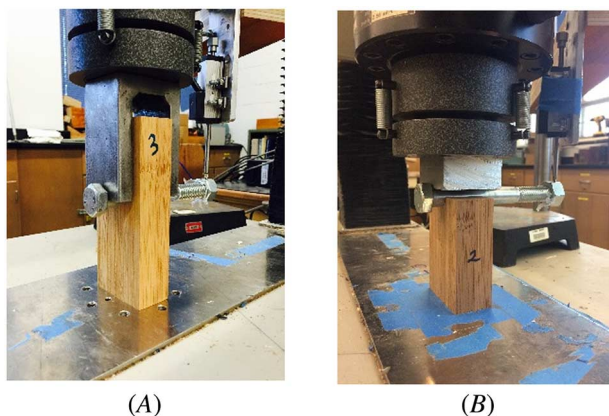
The LVB were specimens measured 152 by 63 by 32 mm<sup>3</sup> and 90 by 63 by 32 mm<sup>3</sup> for full- and half-hole specimens, respectively. Using a 17.5 mm (11/16th inch) diameter drill bit, a hole was drilled in the middle of the block to accommodate a 15.9 mm (5/8th inch) diameter steel (grade 5.5) bolt. As the finished drilled surface was smooth and even, the hole was not reamed. A different steel loading apparatus was used for the full- and half-hole specimens to ensure the application of the load onto the wood contact surface follows the standard. Per the standard, a crosshead rate of 1 mm/min was used to produce failure between 1–10 minutes. The test was conducted in displacement control mode, and the displacement directly beneath the contact zone was obtained by means of an LVDT (see fig. 2).

## Embedment Test Results

The embedment test results, shown in Table 1, reveal the stiffness at the contact surface, which in turn leads to finding the local modulus of elasticity (MOE) in the contact zone.

**FIG. 2**

Embedment test setup: displacement was measured in contact zone for (A) full-hole and (B) half-hole specimens.



In **figure 3**, representative curves for full- and half-hole tests are shown where the difference in the load-bearing capacity of LVB from each test is noticeable. Although the measured embedment yield load in the half-hole arrangement is higher than that of the full-hole, fracture occurs at approximately the same displacement for both. The rationale behind this phenomenon will be explained in a later discussion section of this article through

**TABLE 1**

Stiffness measured at contact surface

	Stiffness at Contact Surface, N/mm	Ultimate Displacement, mm	Yield Load (%5 Dowel Diameter), kN	Embedment Strength Parallel to Grain, MPa
Full-Hole Test				
Mean	32,400	1.18	27.1	34.4
CV	5.6 %	24 %	8 %	8 %
Half-Hole Test				
Mean	45,900	1	28.8	36.6
CV	15 %	25 %	10 %	10 %

Note: CV = Coefficient of variation.

**FIG. 3**

Load-bearing capacity comparison between full- and half-hole LVB dowel joints (displacement control mode).

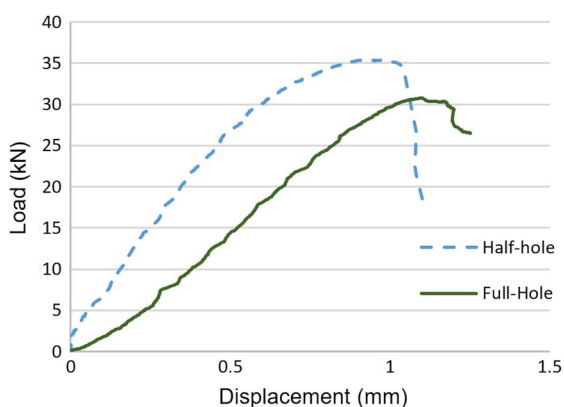


**FIG. 4**

Splitting failure in LVB dowel joint when loaded parallel to the grain:  
(A) full- and (B) half-hole.



FE results. **Figure 4** illustrates the failure of the full- and half-hole dowel joints after being loaded in compression parallel to the grain up to their maximum stress.

For the full-hole test, in 80 % of the specimens, the crack started and continued to grow at between 4 to 4.7 mm off-center (i.e., lower 1/6th of the hole perimeter) and in 20 % of the specimens, an on-center crack was also detected beneath the loaded area. These tests suggest that a combination of tension perpendicular to the grain and shear stresses on the specimen is responsible for failure.

For the half-hole test, on the other hand, the fracture consistently occurred off-center in the lower 1/6th of the hole perimeter (see **fig. 3B**), which suggests that shear stress (only) is the primary cause of failure.

## FE Model

To find a more detailed explanation of the different failure behavior of the LVB dowel joints in full- and half-hole setup, a nonlinear three-dimensional FE model was built using ANSYS Mechanical APDL17.2 (ANSYS, Inc., Canonsburg, PA). The two test setups described in ASTM **D5764** (full- and half-hole) were followed explicitly.

The model was developed with hexahedra homogenous 20-node elements (SOLID186) to investigate the stress distribution and clarify the cause of failure in each test method. Displacement-controlled compressive loading was applied to the steel bolt, and the specimen model was fixed at the bottom. The bolt hole diameter was modeled as 1/16th inch larger than the bolt diameter to reflect realistic building practice as specified in the National Design Specification for Wood Construction.<sup>13</sup> Because of symmetry, half of the dowel was modeled and symmetric planes were restricted in the direction normal to the plane of symmetry. Mesh refinement was performed in the area of interest around the bolt hole. The number of elements used in the models are 6,142 and 4,186 for the full- and half-hole models, respectively.

Contact elements (CONTA174 and TARGE170) were employed to create flexible surface-to-surface contact for the steel bolt and LVB hole. Then, an augmented Lagrange algorithm was used to solve the contact problem, implementing parameter  $FKN=0.1$  to adjust the contact stiffness in the contact area. The other important contact parameter is contact tolerance ( $FTOL$ ), which is the minimum distance that the program searches for contact, and calculates contact force with a lower computer cost. The  $FTOL$  parameter is important because choosing proper contact tolerance, together with proper load increment, leads to converged and more accurate results. For our work, after choosing different values (given in **Tables 2** and **3**)  $FTOL$  was considered as 0.15 and 0.01 for the full- and half-hole models, respectively. Finally, value 0.2 for the coefficient of friction between the LVB and steel dowel was chosen.<sup>2</sup>

### CONTACT MODELING

To define the most efficient mesh at the contact area and decrease the amount of unrealistic penetration, there are two things that should be considered:

**TABLE 2**

Full-hole model calibration results

FE Model	Mesh Size, mm	Model		Constraint Method	Results
		<i>FKN</i>	<i>FTOL</i>		Contact Stiffness in Elastic Zone, K, N/mm
1	1	0.1	0.15	Penalty	31,300
2	1	0.1	0.15	Augmented	31,500
3	1.5	N/A	0.1	Lagrange	38,800
4	1.5	0.1	0.15	Augmented	<u>32,000</u>
5	1.5	0.1	0.1	Augmented	34,300

**TABLE 3**

Half-hole model calibration results

FE Model	Mesh Size, mm	Model		Constraint Method	Results
		<i>FKN</i>	<i>FTOL</i>		Contact Stiffness in Elastic Zone, K, N/mm
1	1	0.1	0.01	Augmented	Not converged
2	1	0.1	0.1	Augmented	39,000
3	1.5	0.1	0.15	Augmented	36,000
4	1.5	0.1	0.05	Augmented	41,000
5	1.5	0.1	0.01	Augmented	<u>43,000</u>

- Choice of contact/target surfaces: considering the target element characteristic and definition, no penetration is allowed between the target element nodes.<sup>14</sup> Hence, the target element is usually selected for modeling a stiffer body, which, in our case, is the steel bolt (see [fig. 5](#)).
- Contact/target surface relative mesh size: a finer mesh was considered for the target surface (steel dowel) to allow a permissible penetration to the contact surface (wood surface) in the FE model (see [fig. 5](#)).

It is notable that—regarding choosing the proper mesh size—because of the C0 continuity (zero degree of continuity) across the contact boundary, the contact force is very sensitive to mesh discretization. It was found that the results change abruptly with mesh refinement, so mesh refinement at the contact boundary does not necessarily lead to converged results.

### MATERIAL MODEL

An orthotropic bilinear material model with hardening was assumed for the Moso LVB, and the constitutive properties were chosen from the experiment results given in [Table 4](#) for the elastic region. To calculate the

**FIG. 5**

The effect of contact area mesh on penetration: contact body with coarser mesh.

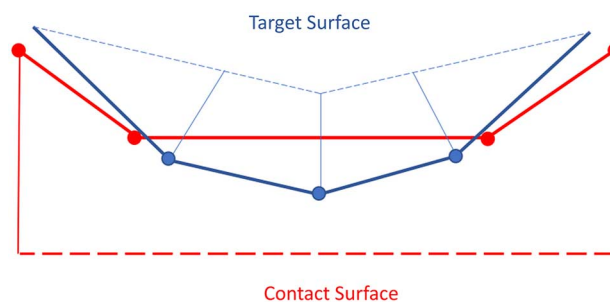


**TABLE 4**

Material properties of Moso LVB

Loading Direction	Density, kg/m <sup>3</sup>	Compression		Tension		Shear
		MOE, MPa	Strength, MPa	MOE, MPa	Strength, MPa	Strength, MPa
Parallel	650	11,600	62	9,219	95	13.15
CV		7 %	3.2 %	15 %	12 %	11 %
Perpendicular	650	1,440	28	200	5.43	–
CV		30 %	11 %	9 %	22 %	

Note: CV = Coefficient of variation.

required parameters for the plastic region—which is defined by yield stress and tangential modulus—the average slope and yield load of 10 embedment tests were used, and the calculated stress and tangential modulus were incorporated in the FE model (reference [fig. 6](#)).

The choice of Poisson ratio and shear modulus values did not affect the stress results noticeably. Hence, they were selected from the literature: the former value being between 0.22–0.25, as noted by Yu et al.,<sup>15</sup> and the latter being 745 MPa, as reported for Moso bamboo.<sup>16</sup> The second and third shear moduli were estimated to be 1/2 and 1/10th (respectively) that of the first shear modulus based on similar mechanical properties for hardwood given in the *Wood Handbook*.<sup>17</sup>

For the steel bolt, the elastic material model was assumed with a yield stress of 210 GPa and Poisson's ratio of 0.3.

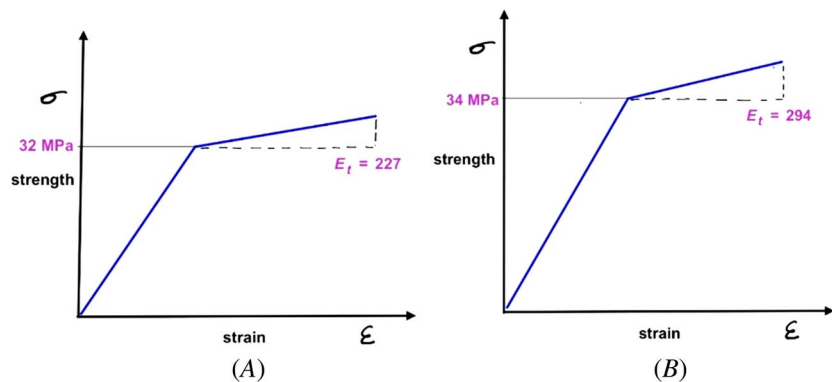
In orthotropic material modeling, care should be taken to choose the right direction of input material properties, especially for the Poisson ratio, to ensure that the stiffness and compliance matrices are positive definite. As a result, the material axes' directions were modeled to coincide with the software global axes and the strongest direction of the LVB, aligned with the global X-axis to avoid any confusion (see [fig. 7](#)).

In both the Lagrange multiplier and penalty methods, the contact is treated as a constraint<sup>14</sup> in structural equilibrium, which is why the contact formulation is independent of the material constitutive models. In this case, the MOE values from the conventional LVB test in [Table 4](#) were used. After running the FE model and achieving the results, for the contact surface validation of our FE model, the contact surface load-displacement curve (in the longitudinal direction) was obtained and compared with the measured load-displacement results by means of an LVDT.

By considering all the aforementioned, the full- and half-hole models were calibrated to the experimental results by considering different combinations of mesh size, load increments, and contact tolerance. The calibration results are presented in [figure 8](#) and [Tables 2](#) and [3](#). Correspondingly, for obtaining the experimental curves shown in [figure 8](#), an LVDT was employed to observe the material load-displacement curve in the midpoint of the contact surface for a

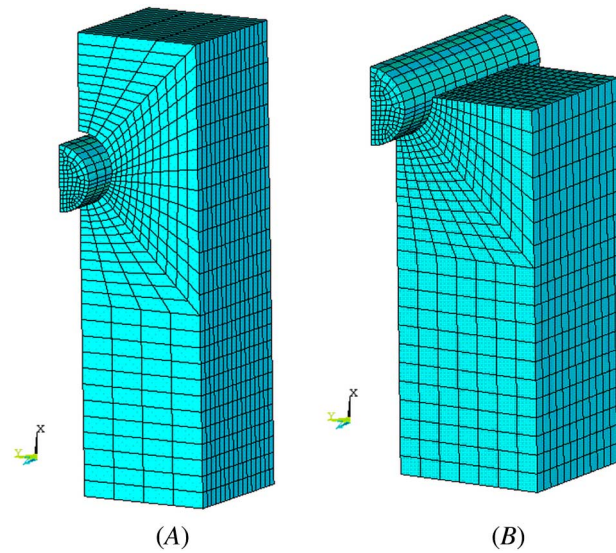
**FIG. 6**

Elastic-plastic material model for full- and half-hole specimens based on embedment test curves: (A) bilinear material model (full-hole) and (B) bilinear material model (half-hole).

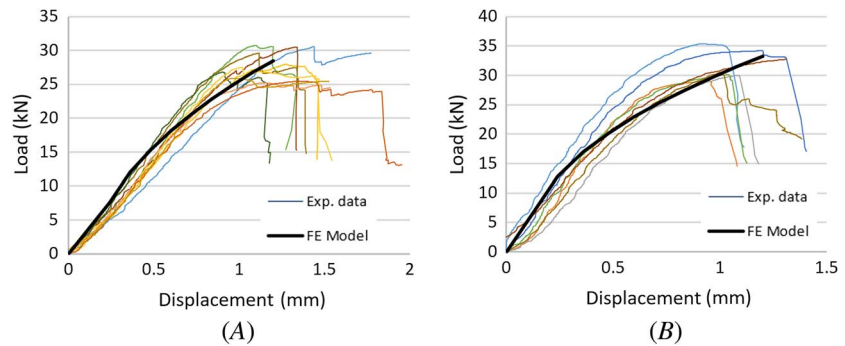


**FIG. 7**

FE model mesh:  
 (A) full-hole model and  
 (B) half-hole model. The  
 strongest direction of  
 LVB is aligned with the  
 global X-axis.

**FIG. 8**

FE model calibration in  
 compressive loading  
 parallel to the grain:  
 (A) full-hole model and  
 (B) half-hole model.



sample size of 10. The measured stiffnesses (i.e., load/displacement) at the contact zone were 32,400 N/mm for the full-hole and 45,500 N/mm for the half-hole specimens in the linear elastic region of the curves.

An initial bulge in the experimental curves was observed, which is the result of self-alignment and self-adjustment between the hole and steel bolt. The applied incremental displacement was increased to 1.2 mm until the LVB dowel joint reached its maximum stress, according to the experimental results in [Table 1](#). A comparison of the FE models and experimental test results in [figure 8](#) led to a verified FE model with an element length of 1.5 mm at the contact edge.

#### LOCAL ELASTIC MODULI EVALUATION

The local elastic modulus ( $E_L$ ) parallel to the grain (needed for the FE model) was determined following an empirical approach that uses the slope of the load-displacement curves of the embedment test. The method is fully explained in the authors' previous work<sup>2</sup>, in which the attained local MOE is calculated based on the dowel geometry and joint stiffness (N/mm). Also, the assumed MOE corresponded to that of the lowest strength direction (i.e., perpendicular to the grain) because, in ANSYS, only one tensile or compressive elastic modulus (independent of material direction) is allowed in the material property input section. The results are summarized in [Table 5](#).

TABLE 5

Calculated local MOE for full- and half-hole models

Test Data Used for Calculations	Sample Size	Failure Load, N		Displacement at Failure, mm		Calculated Local MOE, MPa	
		Full-Hole	Half-Hole	Full-Hole	Half-Hole	Full-Hole	Half-Hole
Parallel to grain (LVB embedment test)	10	28,197	35,100	1.18	1	1,007	1,400
Perpendicular to grain (LVB tension test)	10	N/A	N/A	N/A	N/A	200	200

## FE Failure Analysis

In this analysis, the validated FE models for the full- and half-hole tests as described earlier, were implemented to study the internal stresses in the LVB joint contact area as the displacement was increased to near failure (1.18 and 1 mm upper limits based on the experimental results of the embedment tests).

It is noted that in some FE models, the contact points may oscillate between an open and closed status. This is called “chattering,” and in our case (shown in [fig. 9](#)), contact chattering occurred at the point of separation between the contact and target surface (LVB and steel dowel). This phenomenon created a singular point at this location that led to false high stresses in this point. They were ignored wherever found in the following analysis.

## FE Analysis Results and Discussion

The predicted maximum tensile stress perpendicular to the grain for the full-hole model (see [fig. 10A](#)) was 4.5 MPa and occurred at 8.5 mm beneath the contact surface. This value is slightly less than the mean tensile stress perpendicular-to-grain strength given in [Table 4](#) (5.4 MPa). The relatively high coefficient of variation of the tensile strength in the experimental results of 22 % would suggest that the tensile stress would be a substantial contributing factor to material failure in the full-hole specimens, particularly for weaker specimens in which the strength is less than the predicted stress of 4.5 MPa. On the contrary, for the half-hole specimen, shown in

FIG. 9

Contact chattering occurs at the point of contact/target separation.

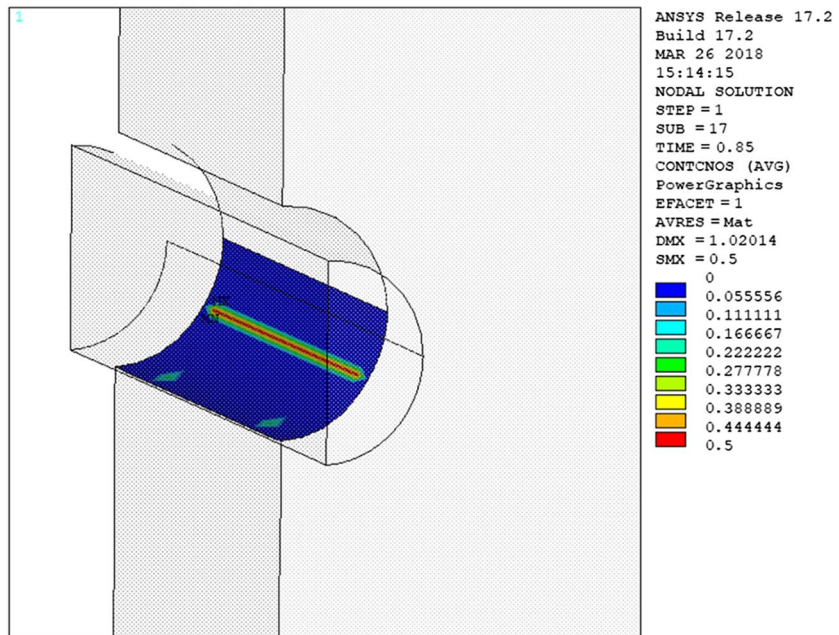


**FIG. 10**

Tensile stress pattern perpendicular to the grain for (A) full-hole model at 1.1 mm loading and (B) half-hole model at 0.9 mm loading.

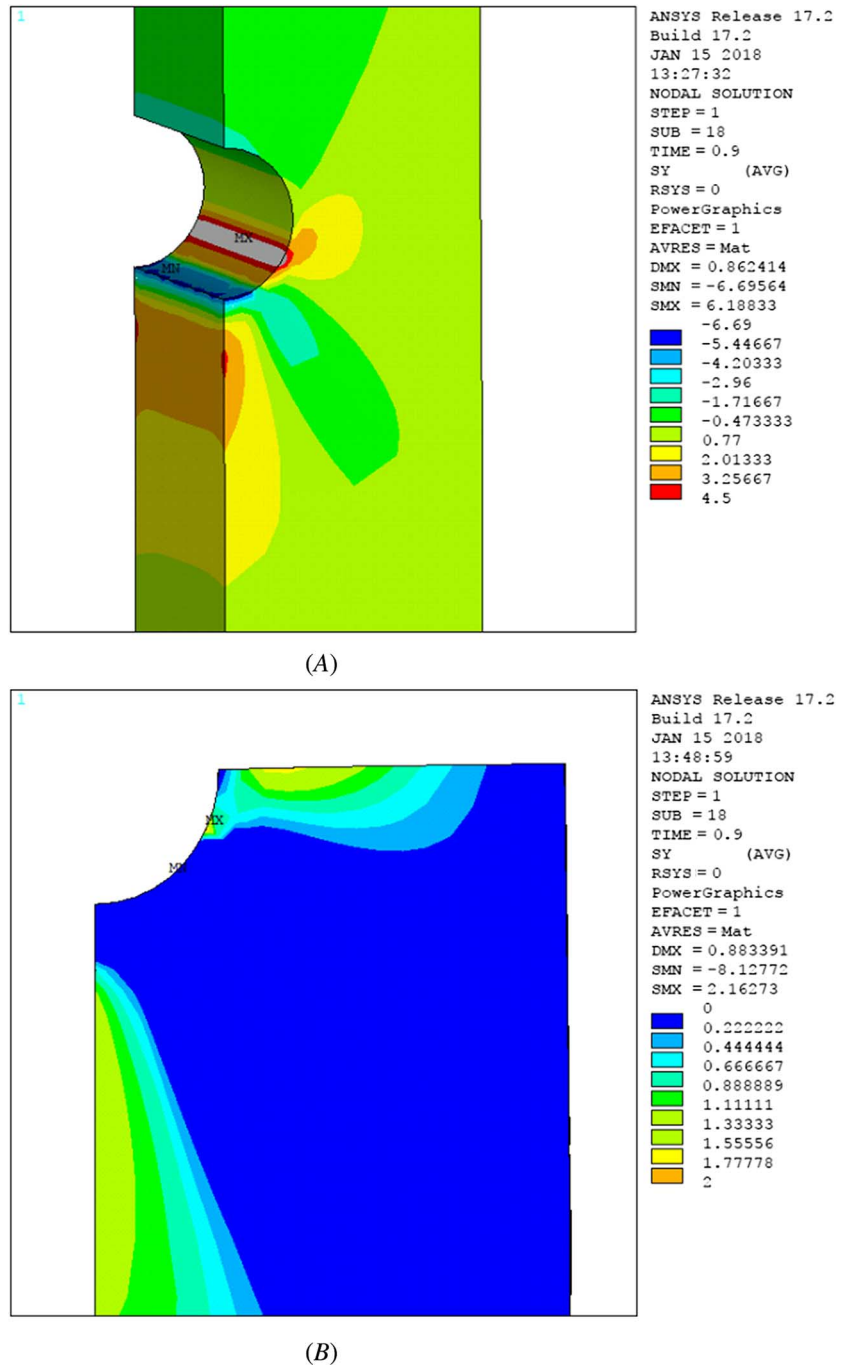
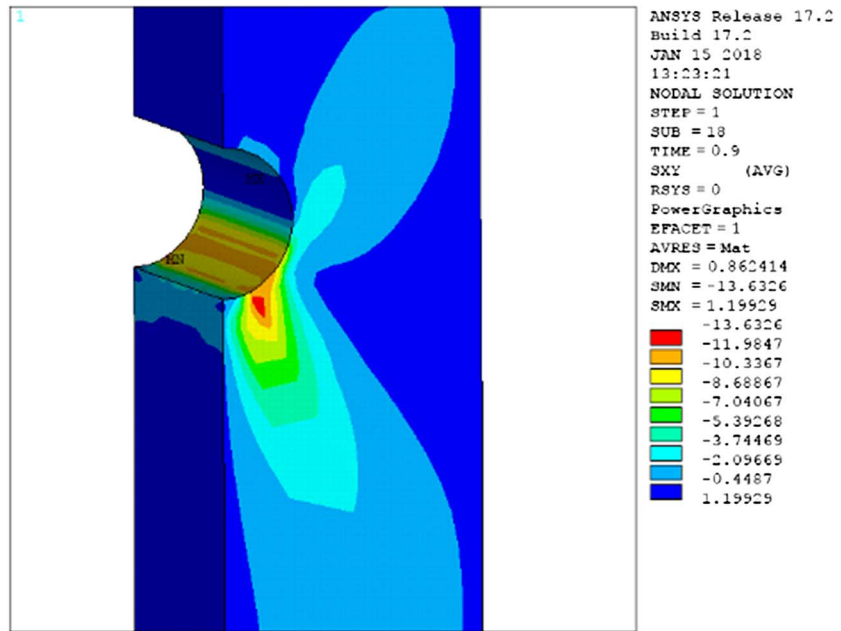


**figure 10B**, the maximum tensile stress reaches only 1.5 MPa (13 mm beneath the contact surface), which is far less than the experimental mean strength of 5.4 MPa and thus would have little contribution to material failure.

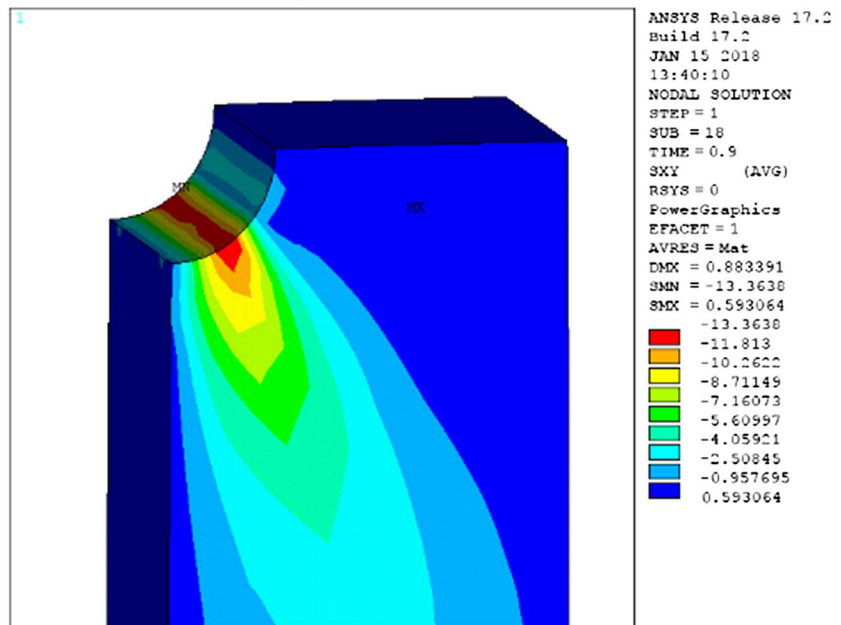
**Figure 11** depicts the maximum in-plane shear stress pattern at failure. In both the full and half-hole models, the maximum shear stress occurs at the lower 1/6th of the hole perimeter, which coincides with the location of the fracture initiation observed in the experiments (see **fig. 4**).

**FIG. 11**

In-plane shear stress pattern for (A) full-hole model at 1.1 mm loading and (B) half-hole model at 0.9 mm loading.



(A)

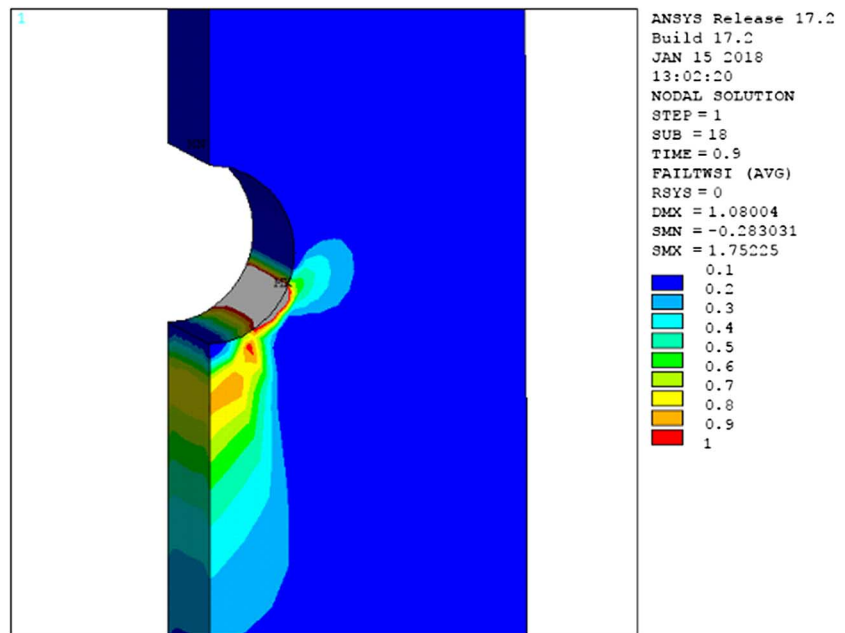


(B)

The FE model for the full-hole specimens indicated that the maximum shear stress reached 13.6 MPa at 1.1 mm displacement (see [fig. 11A](#)), which corresponds well with the experimental shear strength of 13.2 MPa at mean 1.2 mm loading (given in [Table 4](#)). For the half-hole specimen, the maximum shear stress was predicted to be 13.3 MPa at 0.9 mm loading (see [fig. 11B](#)) compared with the experimental value of 13.2 MPa at mean 1.0 mm loading. Both the experimental and FE models confirmed that the half-hole specimens fail at less displacement than the full-hole specimens.

**FIG. 12**

Full-hole model at 1.1 mm loading: (A) Tsai–Wu failure criteria compared with (B) actual failure pattern.



(A)

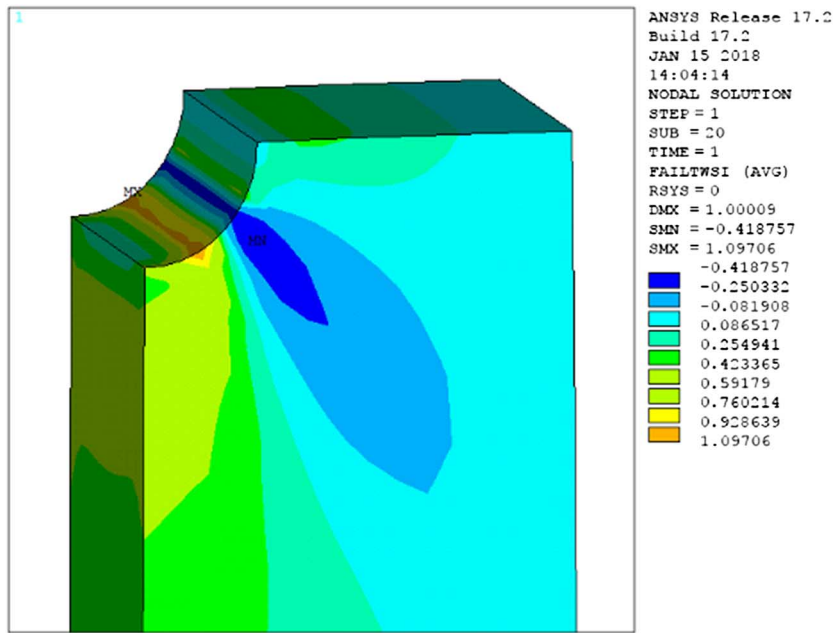


(B)

The Tsai–Wu failure criteria was employed to predict the insipient failure location based on a combined stress state of shear and tensile stress perpendicular to the grain. This criterion is a general quadratic interaction equation in which the failure surface is in the form of a tensor polynomial:

**FIG. 13**

Half-hole model at 1 mm loading: (A) Tsai–Wu failure criteria compared with actual (B) failure pattern.



(A)



(B)

$$F_i \sigma_i + F_{ij} \sigma_i \sigma_j = 1 \text{ for } i, j = 1, 2, \dots, 6 \tag{1}$$

where:

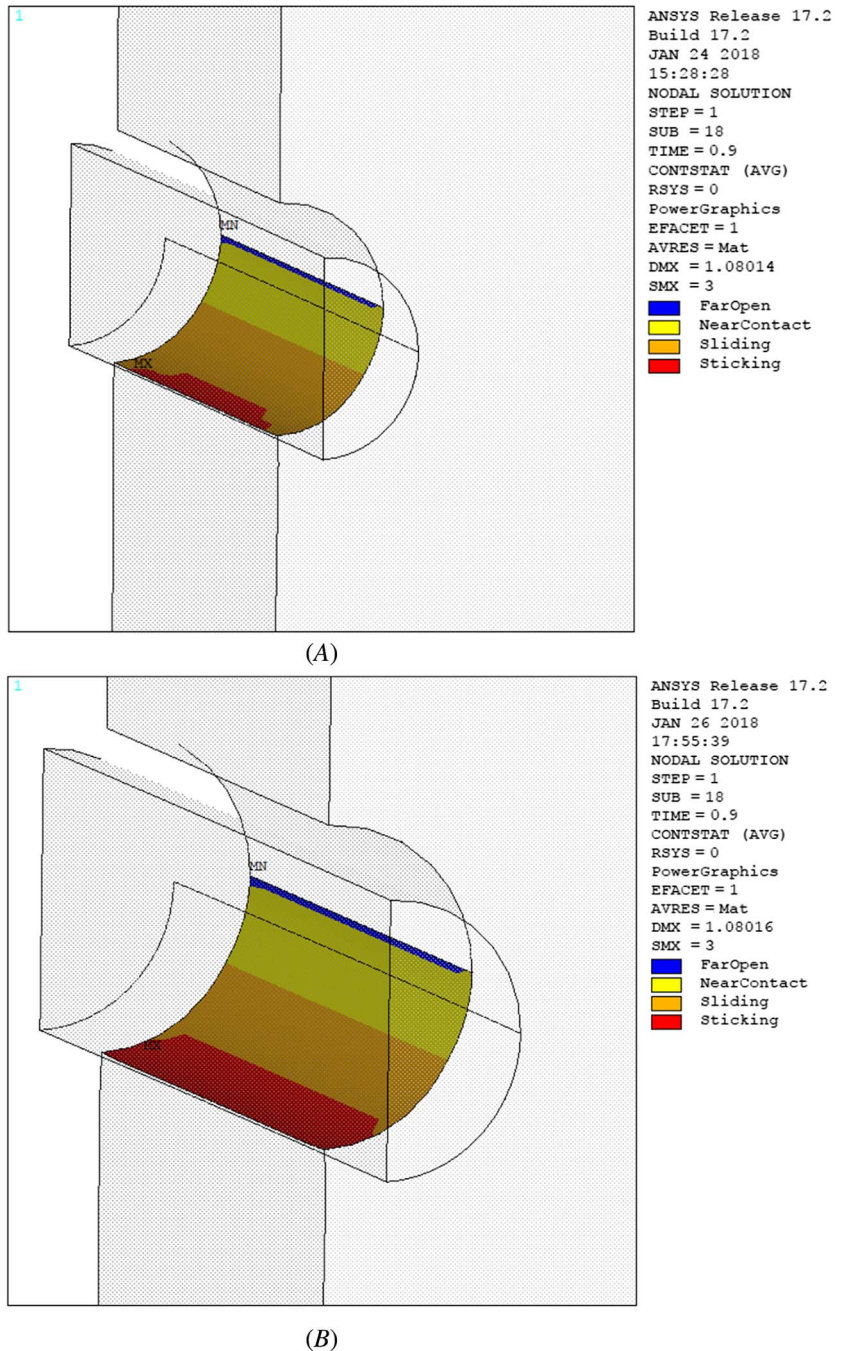
$F_i$  = first rank stress tensor, and

$F_{ij}$  = fourth rank stress tensor.

$F$  parameters are experimentally determined and can be expressed in the terms of uniaxial and shear strength except for  $F_{12}$ , which needs a biaxial test to be determined. Hence, when applying the Tsai–Wu failure criteria, these  $F$  parameters were requested through the ANSYS dialogue box:

**FIG. 14**

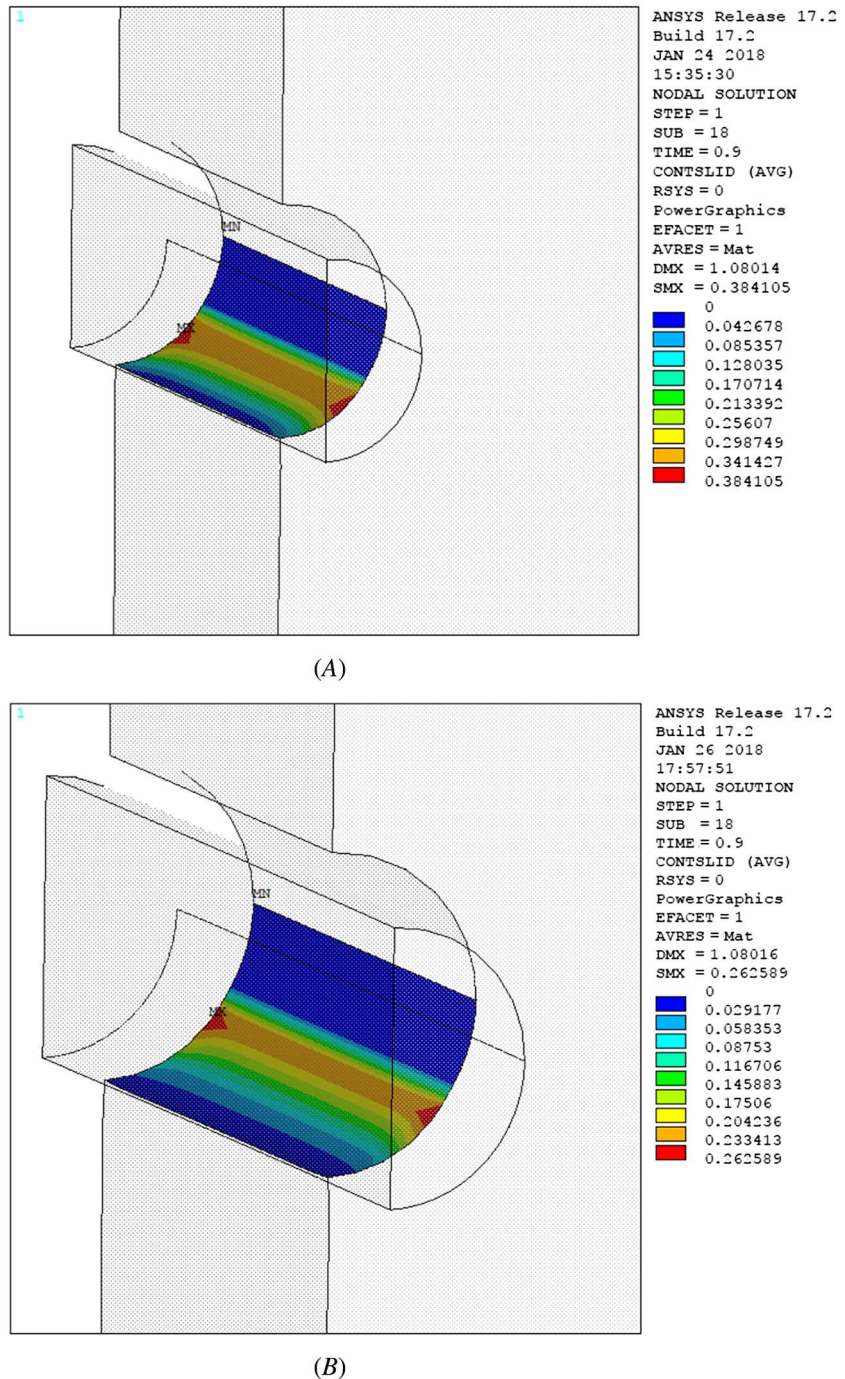
Contact status at 1.1 mm displacement for  
(A)  $\mu = 0.2$  and  
(B)  $\mu = 0.4$ .



- Longitudinal and transverse tensile strength (obtained from [Table 4](#)).
- Longitudinal and transverse compressive strength (obtained from [Table 4](#)).
- Longitudinal and transverse shear strength (obtained from [Table 4](#)).
- Stress coupling coefficient (XY, YZ, XZ): This parameter equals  $2F_{ij}$  in ANSYS nomenclature. The value  $F_{ij}$  was assumed to be 0.00012 using the off-axis tension test data on Glubam, a laminated bamboo product.<sup>18</sup>

**FIG. 15**

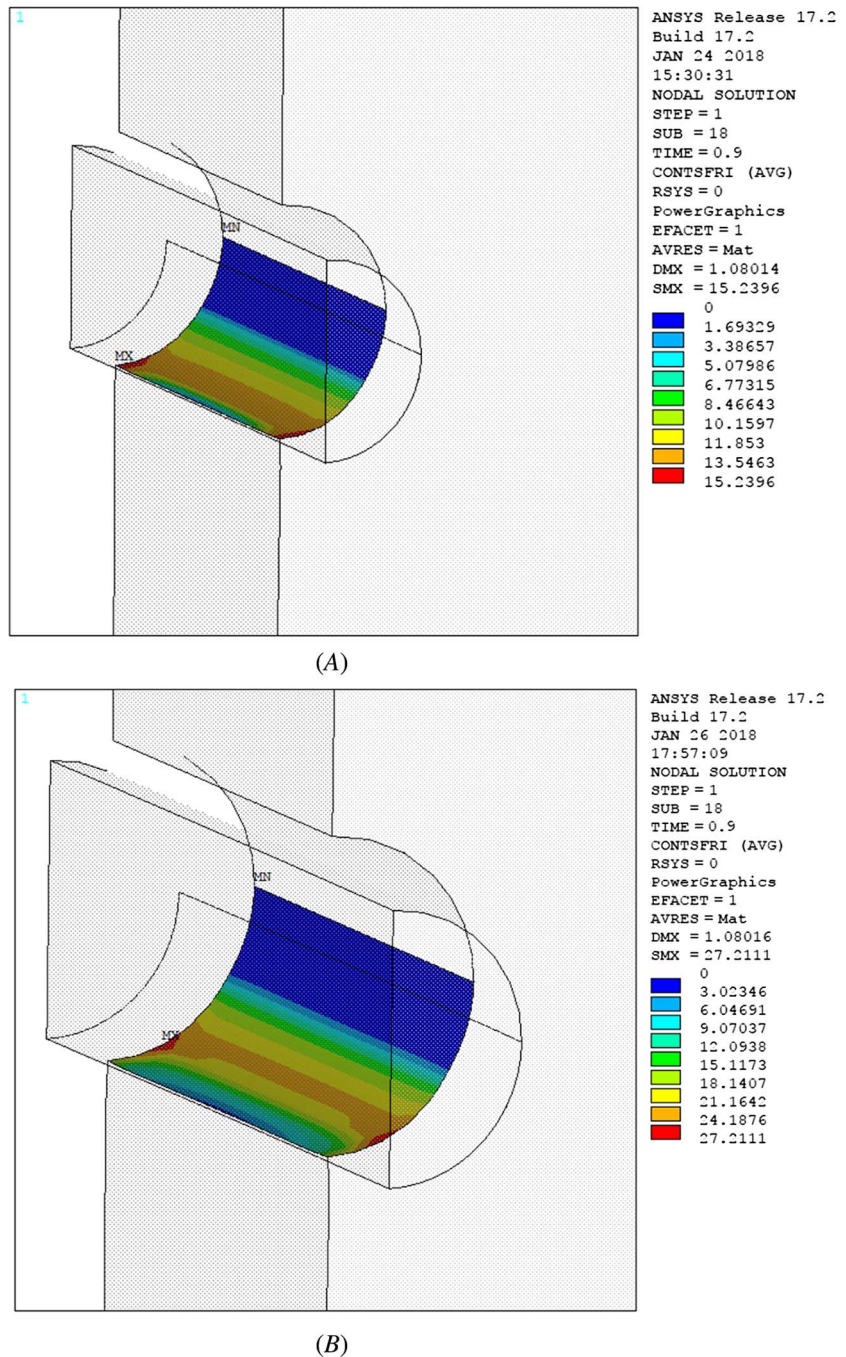
Contact sliding distance at 1.1 mm displacement for (A)  $\mu = 0.2$  and (B)  $\mu = 0.4$ .



Figures 12 and 13 show how the Tsai–Wu criteria effectively predict the location of insipient failure. In figure 12A (after disregarding the value at a singularity due to contact chattering), it is shown that the full-hole model fails at 1.1 mm loading, and the most probable failure area includes the central lower part

**FIG. 16**

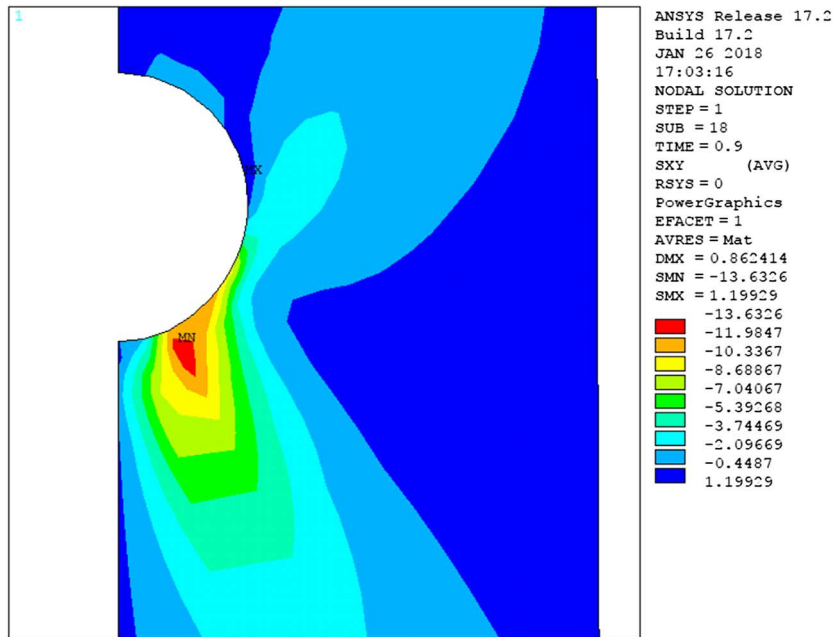
Contact frictional stresses at 1.1 mm displacement for (A)  $\mu = 0.2$  and (B)  $\mu = 0.4$ .



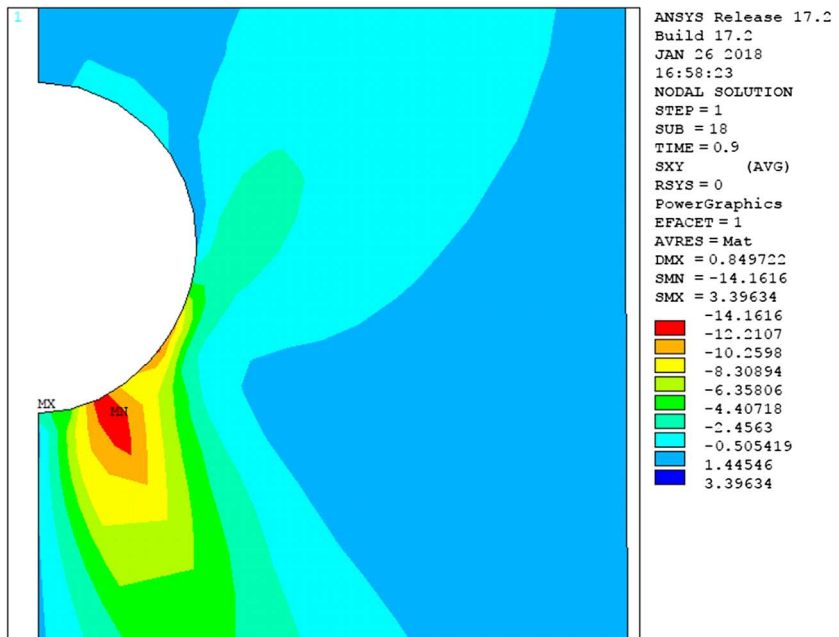
up to the lower 1/6th of the hole perimeter. While in the half-hole model (see [fig. 13A](#)), the failure location is predicted to be just off-center and at the lower 1/6th of the hole perimeter. Considering these results, the Tsai–Wu criteria appears to be a good measure to predict the failure of the LVB dowel joint.

FIG. 17

Shear stress pattern at  
1.1 mm displacement for  
(A)  $\mu = 0.2$  and  
(B)  $\mu = 0.4$ .



(A)



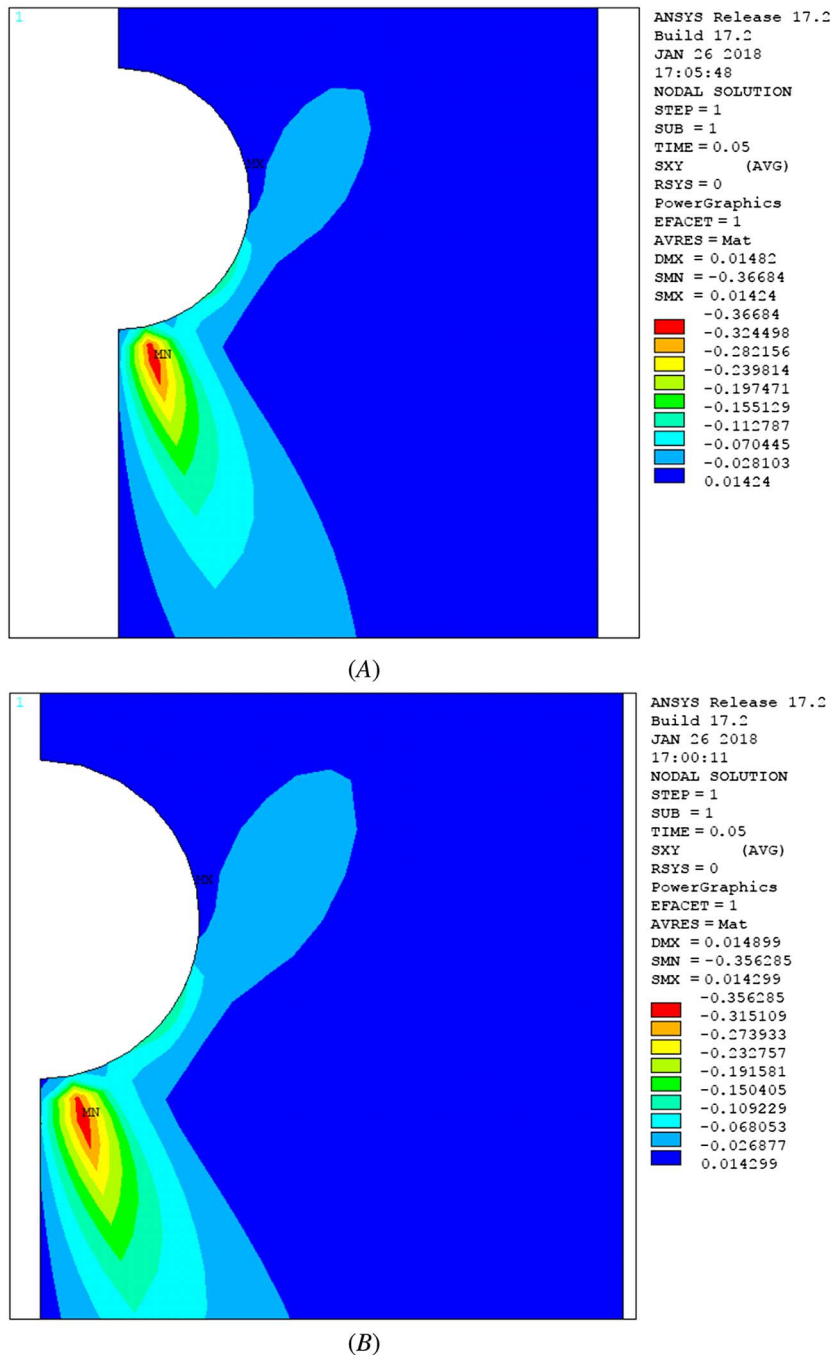
(B)

## Frictional Stresses in the Contact Zone

Sjödin, Serrano, and Enquist<sup>10</sup> showed that, for softwood species, roughening the surface area of the dowel increases shear stresses and decreases tensile stresses in the perpendicular-to-grain direction. And, since tensile stresses

**FIG. 18**

Shear stress pattern at  
0.1 mm displacement for  
(A)  $\mu = 0.2$  and  
(B)  $\mu = 0.4$ .



perpendicular to the grain are the dominant factor in defining the strength of wood specimens, they suggest that designing dowel joints with a rough contact surface ( $0.3 < \mu < 0.5$ ) improves the load-bearing capacity.

Given that in the LVB dowel joint (which is arguably similar to a hardwood species) the determining factor of the load-bearing capacity is shear stress, the effect of a friction coefficient on the shear stress results are of

particular interest. Consequently, two FE models of dowel joints are considered here: one with  $\mu = 0.2$  and the other with  $\mu = 0.4$ .

Both models are the same in the terms of material properties and boundary conditions, except for the coefficient of friction. **Figure 14**, which represents the contact status in both models, shows that the FE model with  $\mu = 0.4$  has a larger area in sticking status for the same applied displacement. This leads to less sliding distance in this model, according to **figure 15**. Consequently, the frictional stresses are much higher in the  $\mu = 0.4$  FE model (see **fig. 16**), which in turn leads to higher shear stresses, as shown in **figure 17**. By increasing the coefficient of friction to 0.4, the maximum shear stress has increased by 4 %, which—compared with the results for softwood species<sup>9</sup>—is not significant. However, it confirms that, in dowel joints with similar size, material, and loading conditions, shear stresses are higher in the dowels with rough contact surfaces. This means that, contrary to wood connections, the smoother contact surface contributes to higher strength of the LVB dowel connections. It is noted that this conjecture should be confirmed in a future study by carrying out experiments on rough and smooth surfaces for LVB material.

**Figure 18** shows shear stresses in the first sub-step of loading in both the frictional models. Since the dowel is still in the sticking status for both models, the shear results are equal in the beginning, and the maximum shear stress is also closer to the centerline. As the loading increases and the steel dowel begins to slide, the location and value of the maximum shear stresses change, depending on the coefficient of friction (see **fig. 15**).

## Conclusion

In this article, two separate methods described in the material testing standard ASTM D5764 for evaluating dowel joints of wood and wood-based products were investigated for LVB material: full- and half-hole specimen procedures. After performing a mixed mode analysis of internal stresses and investigating the LVB fracture behavior in experiments, both FE and experimental analysis revealed a noticeable difference between the failure behavior of the LVB full- and half-hole dowel joints: for the full-hole specimen, a combination of shear stresses (as the main cause of failure) and tensile stresses perpendicular to the grain (as a secondary cause of failure) were responsible, while for the half-hole specimens, shear stresses parallel to the grain dominated failure.

It was also shown, both numerically and experimentally, that for the same applied displacement, the half-hole specimen failed at slightly less displacement than the full-hole specimens, despite a higher load-bearing capacity and stiffness. This is because the higher internal shear stresses exceeded the LVB shear strength sooner than in the full-hole specimen. This suggests that higher dowel stiffness and load-bearing capacity does not lead to stronger joint design for displacement-based loading.

In view of all aforementioned, the authors recommend that only the full-hole specimen test procedure be used to evaluate LVB dowel joint behavior, as it more closely represents real-life connection conditions.

It has been advised in the literature to incorporate the frictional property of the dowel in the standard dowel test methods. This is because the findings for timber show that the smoother frictional surface in the dowel joints leads to lower strength and vice versa. Contrary to this finding, as was mentioned in this article, since the failure mechanism of the LVB dowel joint is different from timber and shear stresses are a determinant factor for strength calculations, further experimental program is suggested to see the importance of surface smoothness in LVB and other engineered wood materials with similar orthotropic properties.

## ACKNOWLEDGMENTS

This work was generously supported by the National Institute of Food and Agriculture, U.S. Department of Agriculture, MAS00026/1000963. The authors would like to thank Mr. Dan Pepin, shop manager of the Building and Construction Technology program at the University of Massachusetts, Amherst, for his contributions to the project.

## References

1. *Standard Specification for Evaluation of Structural Composite Lumber Products*, ASTM D5456-17e1 (West Conshohocken, PA: ASTM International, approved 2017).
2. T. P. Reynolds, B. Sharma, K. Harries, and M. Ramage, "Dowelled Structural Connections in Laminated Bamboo and Timber," *Composites Part B: Engineering* 90 (April 2016): 232–240, <https://doi.org/10.1016/j.compositesb.2015.11.045>
3. N. Khoshbakht, P. L. Clouston, S. R. Arwade, and A. C. Schreyer, "Computational Modeling of Laminated Veneer Bamboo Dowel Connections," *Journal of Materials in Civil Engineering* 30, no. 2 (2018): 1–11, [https://doi.org/10.1061/\(ASCE\)MT.1943-5533.0002135](https://doi.org/10.1061/(ASCE)MT.1943-5533.0002135)
4. C. L. Santos, A. M. P. de Jesus, J. J. L. Morais, and J. L. P. C. Lousada, "A Comparison between the EN 383 and ASTM D5764 Test Methods for Dowel-Bearing Strength Assessment of Wood: Experimental and Numerical Investigations," *Strain* 46, no. 2 (2010): 159–174, <https://doi.org/10.1111/j.1475-1305.2008.00570.x>
5. *Timber Structures. Test Methods. Determination of Embedment Strength and Foundation Values for Dowel Type Fasteners*, BS EN 383:2007 (Brussels: European Committee for Standardization, approved 2007).
6. *Standard Test Method for Evaluating Dowel-Bearing Strength of Wood and Wood-Based Products*, ASTM D5764-97a (West Conshohocken, PA: ASTM International, approved 2018).
7. S. Franke and N. Magniere, "Discussion of Testing and Evaluation Methods for the Embedment Behaviour of Connections" (paper presentation, International Network on Timber Engineering Research, Bath, UK, September 1–4, 2014).
8. P. D. Rodd, "The Analysis of Timber Joints Made with Circular Dowel Connectors" (PhD thesis, University of Sussex, 1973).
9. A. J. M. Jorissen, "Double Shear Timber Connections with Dowel Type Fasteners," *Heron* 44, no. 3 (1999): 0046–7316.
10. J. Sjödin, E. Serrano, and B. Enquist, "An Experimental and Numerical Study of the Effect of Friction in Single Dowel Joints," *Holz als Roh- und Werkstoff* 66, no. 5 (2008): 363–372, <https://doi.org/10.1007/s00107-008-0267-z>
11. *Standard Test Methods for Small Clear Specimens of Timber*, ASTM D143-09 (West Conshohocken, PA: ASTM International, approved 2009). <https://doi.org/10.1520/D2915-98E01>
12. *Standard Practice for Evaluating Allowable Properties for Grades of Structural Lumber*, ASTM D2915-98e1 (West Conshohocken, PA: ASTM International, approved 1998).
13. *National Design Specification for Wood Construction*, NDS (Leesburg, VA: American Wood Council, approved 2015).
14. N.-H. Kim, *Introduction to Nonlinear Finite Element Analysis* (New York: Springer, 2015).
15. Y. Yu, G. Tian, H. Wang, B. Fei, and G. Wang, "Mechanical Characterization of Single Bamboo Fibers with Nanoindentation and Microtensile Technique," *Holzforschung* 65, no. 1 (2011): 113–119.
16. S. Askarnejad, P. Kotowski, F. Shalchy, and N. Rahbar, "Effects of Humidity on Shear Behavior of Bamboo," *Theoretical and Applied Mechanics Letters* 5, no. 6 (2015): 236–243, <https://doi.org/10.1016/j.taml.2015.11.007>
17. United States Department of Agriculture, Forest Service, Forest Products Laboratory, "Mechanical Properties of Wood," in *Wood Handbook: Wood as Engineering Material* (Madison, WI: United States Department of Agriculture, 2010), 5–44.
18. R. Z. Yang, Y. Xiao, and F. Lam, "Failure Analysis of Typical Glulam with Bidirectional Fibers by Off-Axis Tension Tests," *Construction and Building Materials* 58 (May 2014): 9–15, <https://doi.org/10.1016/j.conbuildmat.2014.02.014>